Macromolecules

ARTICLE

pubs.acs.org/Macromolecules

Structure−Property Relationships of Nanocomposites Based on Polypropylene and Layered Double Hydroxides

Purv J. Purohit,[†] Jesús E. Huacuja-Sánchez,[†] De-Yi Wang,[*,‡,§] Franziska Emmerling,[∥] Andreas Thünemann,[∥] Gert Heinrich,[‡,⊥] and Andreas Schönhals[*,†]

[†]BAM Federal Institute for Materials Research and Testing, Unter den Eichen 87 12205, Berlin, Germany

[‡]Leibniz Institute of Polymer Research Dresden, Hohe Strasse 6, 01069 Dresden, Germany

[§]Center for Degradable and Flame-Retardant Polymeric Materials (ERCEPM-MoE), College of Chemistry, Sichuan University, Chengdu 610064, China

[∥]BAM Federal Institute for Materials Research and Testing, Richard Willstätter Str. 11, 12489 Berlin, Germany

[⊥]Institut für Werkstoffwissenschaft, Technische Universität Dresden, 01069 Dresden, Germany

ABSTRACT: Nanocomposites based on polypropylene (PP) and organically modified ZnAl layered double hydroxides (ZnAl-LDH) were prepared by melt blending and investigated by a combination of differential scanning calorimetry (DSC), small- and wide-angle X-ray scattering (SAXS and WAXS), and dielectric relaxation spectroscopy (DRS). An average number of stack size of LDH layers is calculated by analyzing the SAXS data which is close to that of pure organically modified ZnAl-LDH. Scanning microfocus SAXS investigations show that the ZnAl-LDH is homogeneously distributed in the PP matrix as stacks of 4−5 layers with an intercalated morphology. DSC and WAXS results show that the degree of crystallinity decreases linearly with the increasing content of LDH. The extrapolation of this dependence to zero estimates a limiting concentration of ca. 40% LDH where the crystallization of PP is completely suppressed by the nanofiller. The dielectric spectra of the nanocomposites show several relaxation processes which are discussed in detail. The intensity of the dynamic glass transition (β-relaxation) increases with the concentration of LDH. This is attributed to the increasing concentration of the exchanged anion dodecylbenzenesulfonate (SDBS) which is adsorbed at the LDH layers. Therefore, a detailed analysis of the β-relaxation provides information about the structure and the molecular dynamics in the interfacial region between the LDH layers and the polypropylene matrix which is otherwise dielectrically invisible (low dipole moment). As a main result, it is found that the glass transition temperature in this interfacial region is by 30 K lower than that of pure polypropylene. This is accompanied by a drastic change of the fragility parameter deduced from the relaxation map.

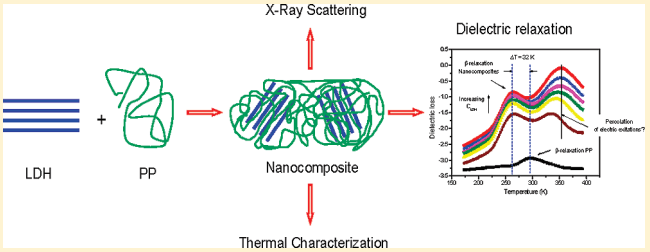

1. INTRODUCTION

Polymer-based nanocomposites are gaining an increasing interest because of the substantial improvements in material properties such as gas and solvent barrier, toughness, mechanical strength, flame retardancy, etc., as compared to micro- or macro-scaled composites.[1−7] The reasons behind these properties improvements are the small size of the filler particles, its homogeneous dispersion on the nanoscale in the polymeric matrix, and thus the length scale of interaction with the polymer segments. Also, due to the small size of the particles, they have a high surface to volume ratio which results in a high volume fraction of an interface area between the polymer matrix and the nanoparticle.[8] The structure, like the packing density and/or the molecular mobility, of the segments in that interface can be quite different from those in the matrix polymer.[9−12] Therefore, the interfacial area between the polymer and the nanofiller is crucial for the properties of the whole composite. This concept of nanocomposites needs to be explored further by establishing reliable models relating the nanostructure and the macroscopic properties. An increasing number of review articles are published on structure−property relationships of polymer nanocomposites (for instance, see refs 13−15).

Various types of fillers are employed for the successful preparation of polymer-based nanocomposites. Among the well-known nanofillers are layered silicates,[1,5,16−18] metal nanoparticles,[19] carbon nanotubes,[20−22] and polyhedral oligomeric silsesquioxanes (POSS).[23−27] Recently, a different class of layered material known as layered double hydroxides (LDH) has attracted great interest.[28−30]

LDHs belong to the general class of anionic clay minerals. The most common naturally occurring LDH is hydrotalcite. LDH materials have a broad range of chemical composition and are well-known for their catalytic activity.[31] Because of a large amount of tightly bound water[32] and synergistic effects, they are able to enhance the flame retardancy of polymeric materials.[33−36]

Received: February 11, 2011
Revised: May 3, 2011
Published: May 11, 2011

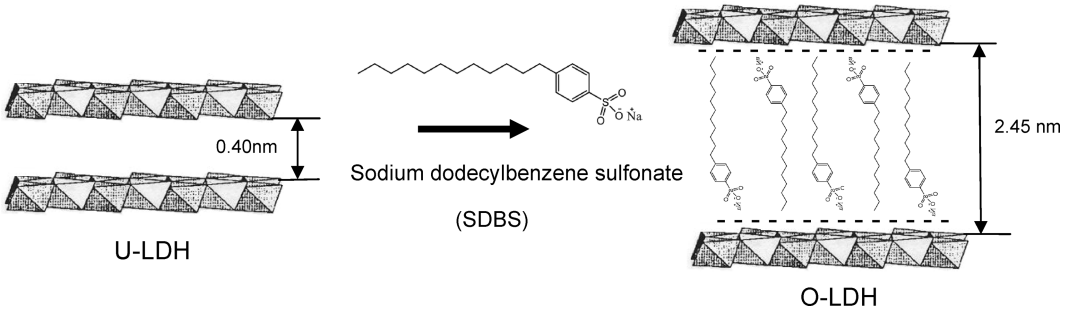

Figure 1. Schematic representation of organically modified ZnAl-LDH (O-LDH), including the structure of SDBS. The numbers mean the interlayer distance between two LDH sheets (the thickness of the LDH sheets is subtracted from the basal spacing).

LDHs have a layered structure like layered silicate clays, but in case of the former the layers are positively charged with anionic interlayer gallery. By employing bulky organic anionic species, the LDH can be modified by the exchange of these interlayer anions. This results in an increase in the distance between the layers, so that polymer chains can intercalate into the gallery and nanocomposites with an intercalated or exfoliated morphology can be obtained.

Recently, various techniques such as X-ray scattering, dielectric spectroscopy,[12,30,37−42] rheology,[43] microscopy, Fourier transform infrared spectroscopy,[44] differential scanning calorimetry,[45] etc., have been employed to investigate the morphology of nanocomposites. For example, Ray and Bandyopadhyay combined X-ray scattering and electron microscopy to quantitatively analyze the nanoclay dispersion in polymer nanocomposites based on poly[(butylene succinate)-*co*-adiapate].[46] Similarly, Bellare et al. quantified the organo-clay dispersion in polypropylene-based nanocomposites using small-angle X-ray scattering.[47] Zhu et al. studied the effect of silica on the chain dynamics of isotactic polypropylene and related it to the mechanical properties of the composite using X-ray scattering and ^{1}H NMR spectroscopy.[48]

In this contribution, the structure−property relationship of nanocomposites based on polypropylene and LDH is investigated by a combination of DSC, SAXS, WAXS, and DRS for the first time. The approach of combining the different characterization techniques involving a variety of different probes will provide different windows to characterize the structure property relationship of this particular system. But this unique combination will be in turn helpful to establish standard models for structure−property relationships of polymer-based nanocomposites in general.

2. EXPERIMENTAL SECTION

2.1. Materials. Layered double hydroxides are anionic clays whose structure is based on brucite-like layers ($Mg(OH)_2$). In the latter case, each magnesium cation is octahedrally surrounded by hydroxyl groups. An isomorphous substitution of Mg^{2+} by a trivalent cation or by a combination of other divalent or trivalent cations occurs in the LDHs. Therefore, the layers become charged and anions between the layers are required to balance the charge. LDH can be represented by the general formula $[M^{II}_{1-x}M^{III}_x(OH)_2]^{x+}\cdot[(A^{n-})_{x/n}\cdot mH_2O]^{x-}$ where M^{II} and M^{III} are the divalent and trivalent metal cations, respectively, and A is the interlayer anion. Examples of divalent ions are Mg^{2+}, Ni^{2+}, and Zn^{2+} and for the trivalent ions are commonly found Al^{3+}, Cr^{3+}, Fe^{3+}, and Co^{3+}. For the present case the LDH material is fully synthetic where the metal cations are Zn^{2+} and Al^{3+}. The intergallery anions employed for the modification of LDH is sodium dodecylbenzenesulfonate (SDBS) whose chemical structure is given in Figure 1.

The metal nitrate salts ($Zn(NO_3)_2\cdot 6H_2O$ and $Al(NO_3)_3\cdot 9H_2O$) and sodium dodecylbenzenesulfonate (SDBS) for the synthesis of organic ZnAl-LDH were obtained from Aldrich and used without further purification. Deionized water was required to dilute the solutions and wash the filtered precipitates. The synthesis of organo-modified ZnAl-LDH was carried out via a one-step method.[54] The typical procedure is the slow addition of a mixed metal (divalent Zn^{2+} and trivalent Al^{3+}) salt solution (with Zn^{2+}:Al^{3+} equal to 2:1) (with MZn^{2+} = 0.025 mol, MAl^{3+} = 0.0125 mol in 200 mL of solution) to a SDBS solution (0.015 mol SDBS in 100 mL of solution) under continuous stirring and maintaining the reaction temperature at 323 K. During the synthesis, the pH value was maintained at 9 ± 0.1 by adding suitable amount of 1 M NaOH solution. The resulting slurry was continuously stirred at the same temperature for 30 min and was allowed to age in a heater at 333 K for 18 h. The final products were filtered and washed several times with distilled water to remove nonreacted surfactant molecules until the pH of the supernatant solution was about 7. The material was then dried in an oven at 343 K until a constant weight was achieved. The product is called organo-modified ZnAl-LDH (O-LDH) where, for comparison, the unmodified ZnAl-LDH (U-LDH) was also synthesized. The empirical formulas both of U-LDH and the O-LDH have been investigated by ICP and elemental analysis. For U-LDH it is $Zn_{0.67}Al_{0.33}(OH)_2(NO_3)_{0.33}\cdot 0.4H_2O$, whereas for O-LDH $Zn_{0.67}Al_{0.33}(OH)_2(SDBS)_{0.28}(NO_3)_{0.05}\cdot 0.4H_2O$ is found. This means SDBS is the only balancing anion. The water content was additionally calculated from TGA measurements to be around 4 wt %, which matches well with the empirical formula. Figure 1 shows the generalized scheme for organic modification of U-LDH.

Polypropylene (PP, homopolymer, HD 120 MO) was purchased from Borealis, Porvoo, Finland. Maleic anhydride grafted polypropylene (MAH-*g*-PP, Exxelor PO1020) as compatibilizer was supplied by Exxon Mobil Chemical.

2.2. Nanocomposite Preparation. The nanocomposites were prepared by a two-step approach. In the first step, the O-LDH was melt-compounded with maleic anhydride grafted polypropylene (MAH-*g*-PP) in a weight ratio of 1:1 (based on the approximate metal hydroxide content of O-LDH) to prepare a masterbatch. In the second step, this masterbatch was added in different amounts to the PP through melt compounding. Both steps were carried out in a corotating twin-screw microextruder (15 mL microcompounder, DSM Xplore, Geleen, The Netherlands). The conditions used for both melt-compounding steps were 463 K with 200 rpm screw speed for 10 min. The concentrations of O-LDH in the nanocomposites were determined based on an approximate metal hydroxide content of the filler. The O-LDH prepared in the present study contains 50% of its weight as metal hydroxide. Table 1 gives the list of prepared samples.

2.3. Characterization Techniques. Dielectric relaxation spectroscopy (DRS) was used to investigate the molecular mobility in the

Table 1. Code and Composition of the Investigated Nanocomposite Samples (Here First and Second Melting Is from DSC Measurement)

sample information		1. melting (1. heating)		crystallization (cooling)		2. melting (2. heating)	
sample code	amount of LDH [wt %]	T_{melt} [K]	ΔH_{melt} [J/g]	T_{crys} [K]	ΔH_{crys} [J/g]	T_{melt} [K]	ΔH_{melt} [J/g]
PP	0	438.7	124	395.9	−111	438.6	117
PP2	2.43	441.5	141	400.1	−112	440.7	114
PP4	4.72	440.2	124	397.9	−106	440.5	110
PP6	6.89	439.8	130	396.9	−100	439.4	105
PP8	8.95	439.3	131	396.0	−96	438.8	101
PP12	12.75	441.4	108	394.5	−86.1	434.9	88.9
PP16	16.20	434.1	97.6	392.6	−74.7	433.7	80.3

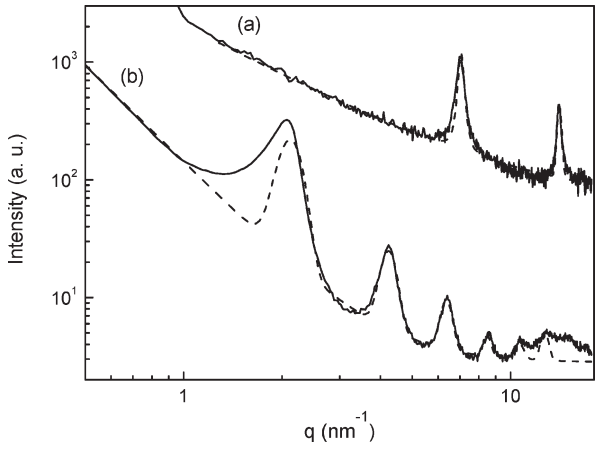

Figure 2. SAXS pattern of unmodified and organically modified LDH (solid lines of (a) and (b), respectively). Dashed lines: sum of Gaussians fitted to the data. The increase of the scattered intensity at low q values was described by a power law.

nanocomposites. DRS is sensitive to fluctuations of molecular dipoles, which can be taken as probe for structure. In case of polymers, it can be related to the molecular mobility of side groups, segments, or the complete chain.[49] A high-resolution ALPHA analyzer (Novocontrol, Hundsagen, Germany) is used to measure the complex dielectric function $\varepsilon^*(f) = \varepsilon'(f) - i\varepsilon''(f)$ (ε' = real part, ε'' = loss part, and $i = \sqrt{-1}$) as a function of frequency f (10^{-1}−10^6 Hz) and temperature T (173−393 K). Samples were prepared in parallel plate geometry. Gold electrodes with a diameter of 20 mm were evaporated on both sides of the samples. Then the samples were mounted between two gold-plated electrodes (20 mm) of the sample holder. All the measurements were done isothermally where the temperature is controlled by a Quatro Novocontrol cryo-system with a stability of 0.1 K. This procedure leads to an effective heating rate of 0.13 K/min. For more details see ref 50.

Thermal analysis was carried out by differential scanning calorimeter (DSC, Seiko Instruments, DSC 220C). The samples (10 mg) were measured from 173 to 473 K with a heating and cooling rate of 10 K/min using nitrogen as protection gas. The enthalpy changes related to melting and crystallization were calculated from 343 to 453 K and 363 to 408 K, respectively.

The SAXS experiments for the nanocomposites were performed at the synchrotron micro focus beamline μSpot (BESSY II of the Helmholtz Centre Berlin for Materials and Energy). Providing a divergence of less than 1 mrad (horizontally and vertically), the focusing scheme of the beamline is designed to provide a beam diameter of 100 μm at a photon flux of 1×10^9 s^{-1} at a ring current of 100 mA. The experiments were carried out employing a wavelength of 1.033 58 Å using a double-crystal monochromator (Si 111). Scattered intensities were collected 820 mm behind the sample position with a two-dimensional X-ray detector (MarMosaic, CCD 3072 × 3072 pixel with a point spread function width of about 100 μm). A more detailed description of the beamline can be found in ref 51. The obtained scattering images were processed and converted into diagrams of scattered intensities versus scattering vector q (q is defined in terms of the scattering angle θ and the wavelength λ of the radiation, thus $q = 4\pi/(\lambda \sin \theta)$) employing an algorithm of the computer program FIT2D.[52]

For the analysis of LDH, X-ray scattering was performed (Figure 2) using a two-circle diffractometer XRD 3003 θ/θ (GE Inspection Technologies/Seifert-FPM, Freiberg) with a Cu Kα radiation (λ = 1.54 Å) generated at 30 mA and 40 kV.

Some morphological analysis was also carried out using transmission electron microscopy (TEM) with microscope LEO 912. The conditions used during analysis were room temperature, 120 kV acceleration voltage, and bright field illumination. The ultrathin sections of the samples were prepared by ultramicrotomy at −120 °C with a thickness of 80 nm.

3. RESULTS AND DISCUSSION

3.1. Characterization of Organically Modified LDH. SAXS was employed to show the modification of LDH by SDBS. The SAXS diagram of the investigated unmodified LDH shows two equidistant reflections at 7.05 and 14.10 nm^{-1} which is characteristic for a layered compound corresponding to a lamellar repeat distance of d = 0.89 nm (Figure 2, upper curve). Here, the thickness of the hydrotalcite brucite-like LDH sheet is 0.49 nm.[53] Subtracting this value gives the effective interlayer distance to be 0.40 nm. Traditionally, indexing LDH powder patterns is based on the hexagonal unit cells although the structures described are mostly rhombohedral; i.e., the peaks were accordingly assigned to the first (003) and second basal reflection (006). We determined peak widths of w = 0.31 nm^{-1} from fitting Gaussian profiles to the measured data (Figure 2, dashed line). The correlation lengths in direction perpendicular to the lamella normal is therefore $l_c = 2\pi/w$ = 20.3 nm. Assuming that lattice distortions could be neglected to a first approximation, this value represents the crystallite thickness in the normal direction of the (00l) plane. Then the average number of layers in a stack in the unmodified LDH is 23.

The modification of the LDH with SDBS to the O-LDH results in a shift of the lamellar reflections toward lower q values, as expected. Six equidistant reflections are clearly visible with the (003) reflection located at 2.14 nm^{-1} corresponding to d = 2.94 nm. This value is in agreement with the value reported recently by Wang et al. (2.98 nm).[54]

dx.doi.org/10.1021/ma200323k |Macromolecules 2011, 44, 4342–4354

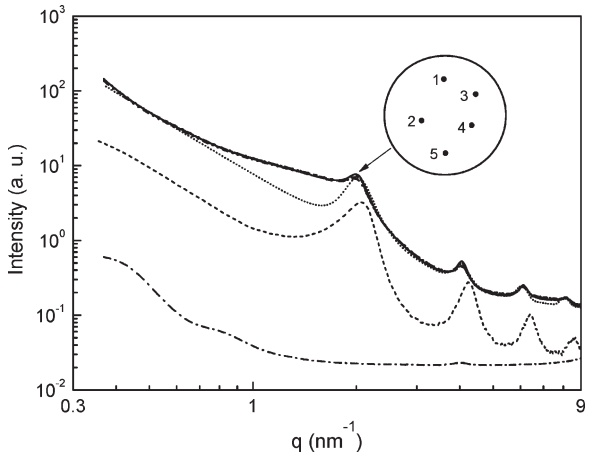

Figure 3. Overlay of five synchrotron SAXS curves from a disk sample of PP16 with a diameter of 30 mm (solid lines). The five positions for SAXS measurements using an X-ray beam size of 0.1 mm were randomly distributed on the disk (inset). Sum of Gaussians were fitted to the data (dotted line). SAXS curves of the O-LDH and the pristine PP (dashed and dash-dotted line, respectively).

Subtraction of the thickness of the brucite-like LDH sheet results in an effective interlayer distance of 2.45 nm for O-LDH. This proves that SDBS is intercalated in the interlayer gallery, thus modifying the LDH. A more detailed discussion of similar systems can be found elsewhere.[54] A peak width of 0.40−0.50 nm^{-1} is determined from fitting six equidistant Gaussians to the experimental curve. Therefore, l_c is in the range of 12.6−15.7 nm, which is equivalent to 4.3−5.3 layers. The number of layers is drastically reduced in O-LDH as compared to U-LDH. This reduction in the number of layers in case of O-LDH can be argued as follows: The SDBS molecules used for the modification increases the *d*-spacing between the layers, which in turn sterically hinders large size stack formation. Moreover, the lack of reflections at 7.05 and 14.10 nm^{-1} in the diagram of O-LDH proves the absence of significant amounts of U-LDH. One has to conclude here that already small stacks of O-LDH with only few layers are used to prepare nanocomposites.

3.2. Homogeneity of the Nanocomposites. The homogeneous distribution of the nanoparticles inside the polymer matrix across the whole macroscopic sample area is essential for the structure−property relationships of nanocomposites. To investigate this for the prepared nanocomposites, SAXS measurements were performed with a microfocus using synchrotron radiation at the μSpotBeamline of BESSY.[51] SAXS were measured at five different positions of the samples having a diameter of more than 30 mm where the spot diameter of the X-ray beam was 0.1 mm. All the individual SAXS pattern collapse into one chart as shown exemplarily for PP16 in Figure 3 (solid curves, positions of measurements at the sample are shown in the inset). The finding of indistinguishable scattering pattern is a strong indication for a homogeneous dispersion of O-LDH in the polymer matrix at a length scale of several centimeters.

An analysis of the data using four equidistant Gaussians with the first maximum at 2.02 nm^{-1} was found to be appropriate (Figure 3, dashed curve). This position corresponds to a lamellar repeat unit of 3.11 nm and hints to a slight expansion of 0.17 nm in comparison to the O-LDH (2.94 nm). A similar expansion of the layer spacing from 2.95 to 3.27 nm has been reported earlier by Costa et al.[28] They interpreted the expansion by partial intercalation of polymer

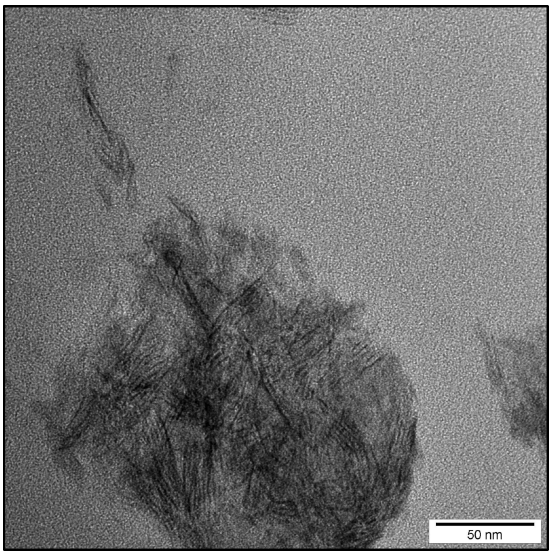

Figure 4. TEM image at a resolution of 50 nm for PP2.

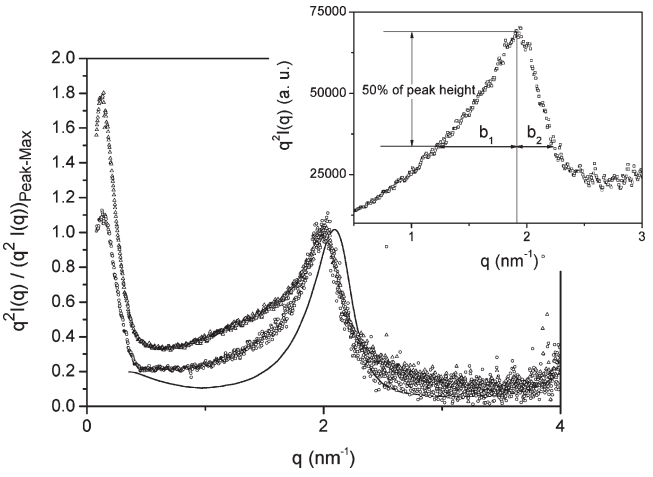

Figure 5. Normalized Kratky plot for O-LDH (solid line) and the nanocomposites PP2 (circles) and PP12 (triangles). The inset shows the low *q* value reflection for PP8 (squares) with the definition of the peak half-width *b* and an asymmetry parameter *w*.

chain segments into the interlayer region of LDH as induced by strong shearing during melting in the extruder.

Peak widths of 0.38−0.50 nm^{-1} are determined from fitting four equidistant Gaussians to the experimental curve. Therefore, l_c is in the range of 12.6−16.5 nm, which is equivalent to 4.05−5.3 layers. This can be also concluded from the TEM image in Figure 4. Stacks of LDH (4−5 layers) are arranged in different orientations in the polymer matrix. For sake of comparison, the scattering of O-LDH and neat PP are displayed in Figure 3 (dashed and dash-dotted curve, respectively). It can be seen that the scattering intensity of PP can be considered as constant for approximation in the region of the appearance of the reflections. The scattering pattern of the samples PP2 to PP12 is similar to PP16 with the same layer spacing and correlation lengths (not shown). Differences are found in the increase of the scattering intensity in the low *q* range, whereas the scattering increases with increasing content of O-LDH. A simple explanation

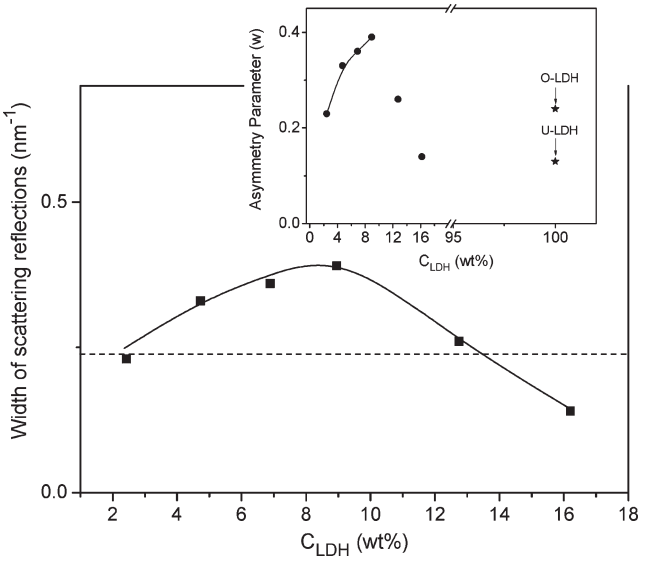

Figure 6. Width of the reflections at lowest q values versus the concentration of LDH. O-LDH (dashed line) is the data value for pure LDH given for comparison. The inset shows the asymmetry parameter as a function of concentration of LDH. The solid line is guide for the eyes.

for this finding is that attractive interactions between neighboring nanoparticles become successively visible at higher LDH content.

It is concluded that the lamellar spacing of the O-LDH increases slightly after incorporation in the PP matrix while the height of the lamellar stack is constant.

In addition to the analysis presented in Figure 3, the peak in Figure 5 is background (pure PP) subtracted and plotted after applying the Lorentz correction $[I(q) \rightarrow q^2 I(q)]$ versus q (Kratky plot). The different data sets are normalized to the maximum peak position for comparison. A closer inspection of the scattering pattern in Figure 5 shows that for the nanocomposites the peak is quite asymmetric. Therefore, to discuss these features in dependence on the concentration of the LDH, the half-width (b) and an asymmetry parameter (w) are defined by using the following equation (see inset of Figure 5):

$$b = b_1 + b_2, \quad w = \frac{b_1 - b_2}{b} \tag{1}$$

Figure 6 shows the change in the width of the low q scattering peaks. As is observed from Figure 5, the peak widths increase asymmetrically. It is worth to note that only a symmetrical broadening of the diffraction peaks can be attributed to a reduction of the stack size. Therefore, the asymmetry of the Bragg peaks must be assigned to another molecular reason. The detailed analysis of the asymmetry parameter gives a result displayed in the inset of Figure 6. As result from the SAXS analysis, it was concluded that around 4−5 layers of LDH per stack are present in the nanocomposite. So, the asymmetry can arise from the arrangement of these stacks in different orientations in the polymer matrix. This can be also observed in the TEM image for (low loading). This line of argumentation seems to be important for low concentration of stacks. For higher concentration these different orientations are averaged out, and the peaks for the samples PP12 and PP16 become more symmetric.

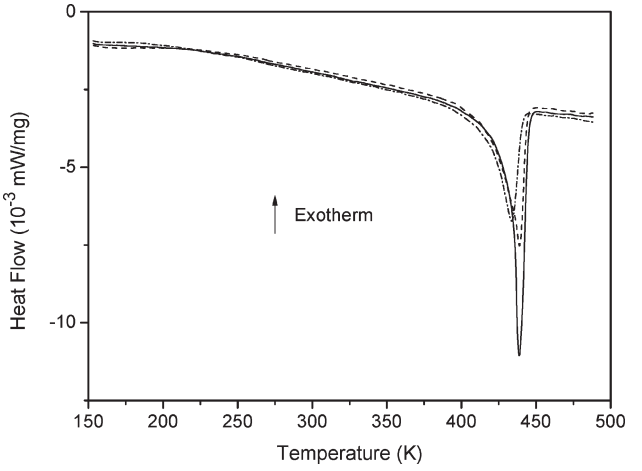

Figure 7. DSC curves for PP and corresponding nanocomposites (second heating run): solid line, PP; dashed line, PP8; dashed-dotted line, PP16. Inset gives the dependence of T_{melt} on the concentration of LDH. The solid line is a guide for the eyes.

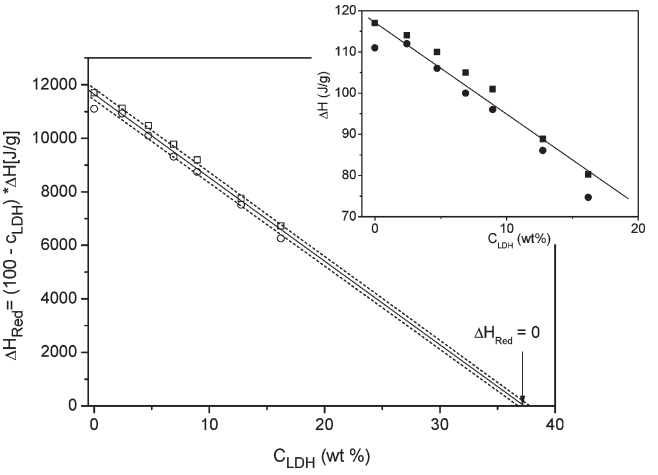

Figure 8. Normalized melting (squares) and crystallization (circles) enthalpies ΔH_{Red} reduced to content of the polymer vs the concentration of LDH. The dashed lines are a linear regression to the melting and crystallization enthalpies. The solid line is a common linear regression to both data sets. The inset shows the melting and crystallization enthalpies vs concentration of LDH. The line is guide for the eyes. For sake of comparison the absolute values of ΔH_{crys} are plotted in the main figure and in the inset as well.

3.3. Crystallinity of the Nanocomposites Using Differential Scanning Calorimetry (DSC) and Wide-Angle X-ray Scattering (WAXS). Figure 7 compares the DSC curves for the second heating run for PP, PP8, and PP16. At higher temperatures, a broad melting transition with a peak at $T_{melt} \sim 438$ K takes place. In the inset of Figure 8 melting (ΔH_{melt}) and crystallization (ΔH_{crys}) enthalpies are plotted versus the concentration of LDH. (For sake of comparison, the absolute values of ΔH_{crys} are plotted.) As expected, both the quantities decrease with increasing concentration of LDH because the amount of polymer decreases with increasing content of LDH. Therefore, the enthalpy values have to be normalized to the content of the polymer. Also, this normalized enthalpy values ΔH_{Red} decreases linearly with increasing concentration of LDH where a similar dependence is obtained for melting and

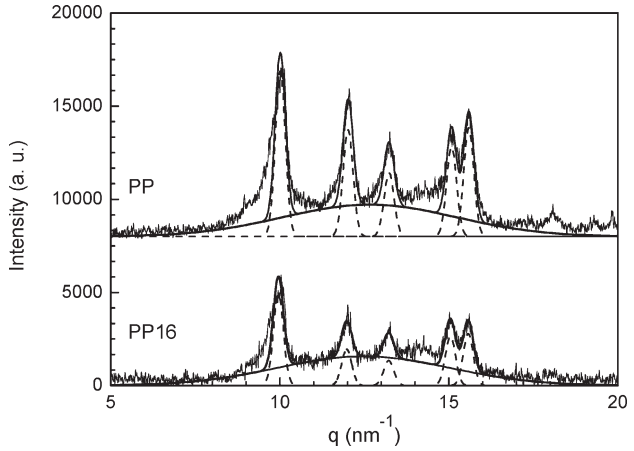

Figure 9. WAXS pattern for the sample PP and PP16 (solid lines in upper and lower curve, respectively). The amorphous contributions are indicated (solid lines) and the crystalline contributions (dashed lines). The degree of crystallinity is 49% (PP) and 31% PP16. For details see the text.

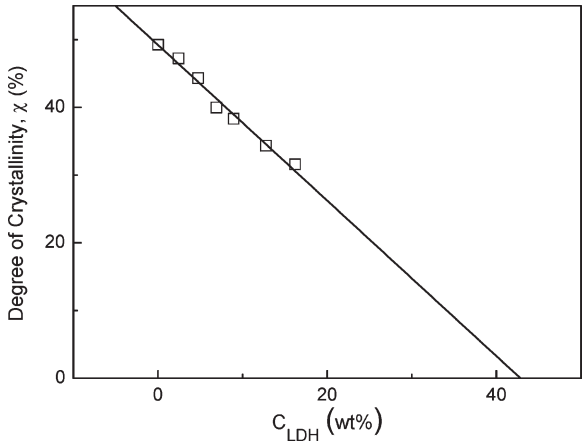

Figure 10. Degree of crystallinity χ vs the concentration of LDH. The solid line is a linear regression to the data.

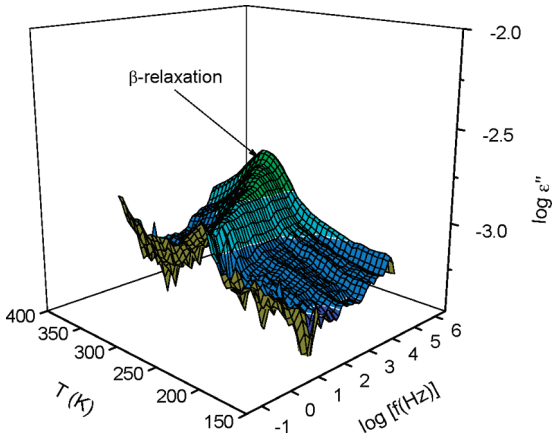

Figure 11. Dielectric loss ε'' of pure PP versus frequency and temperature in a 3D representation.

crystallization. Taking the enthalpy values as a measure for the degree of crystallization, this indicates that the degree of crystallization decreases with increasing the content of LDH. The extrapolation of normalized enthalpy to zero value results in a critical concentration of LDH ca. 40 wt %. For concentrations above this value, the crystallization of PP will be completely suppressed, as the nanoparticles can act as defects and hinder the crystallization of PP segments. The same was observed for nanocomposites based on polyethylene containing LDH[30] and nanocomposites made from polyamide and silica.[45] A similar analysis is reported by Lonjon et al. where they studied the decrease in crystallinity of poly(vinylidene difluoride−trifluoroethylene) as a function of gold nanowires content.[55] Unfortunately, the limiting value of 40 wt % LDH for crystallization cannot be proved experimentally as it is difficult to prepare nanocomposite sample with such a high concentration of nanofiller.

It should be noted that for other systems an increase of crystallization rate and also more perfect crystals were observed for low concentration of nanofiller because the nanoparticles can act as additional nucleation sites.[56,57] So the observed behavior might depend on the type of system studied. For more details the readers are referred to these publications.

In addition to DSC, WAXS is employed to estimate the degree of crystallinity for the nanocomposites directly. The observed dependence on the concentration of LDH estimated by WAXS can be compared with the data obtained from the DSC experiments. The measured WAXS pattern is due to both contributions of the amorphous and crystalline polypropylene. Therefore, the values for the degree of crystallinity χ were determined through a crystalline and amorphous peaks deconvolution process using the software OriginPro, release 8.5, and its *Peak Fitting* tool. Peaks deconvolution was performed using Gaussian functions to obtain the crystalline and amorphous areas ($I_{\text{crystalline}}$ and $I_{\text{amorphous}}$, respectively). The χ values were determined with these areas by using the relation between the total area of the crystalline peaks and the total area of the diffractogram:

$$\chi = \frac{I_{\text{crystalline}}}{I_{\text{crystalline}} + I_{\text{amorphous}}} \times 100\% \qquad (2)$$

Figure 10 shows that χ decrease with increasing concentration of LDH. The result is in good agreement with the DSC results. The extrapolation of the χ to zero gives a concentration of ca. 42 wt % of LDH where there are no crystallites present in the polymer. This limiting value estimated from WAXS measurements is approximately equal to the value obtained by DSC (40 wt %). This can be considered as a strong conclusion due to the fact that both the techniques DSC and WAXS measure slightly different aspects of the same material's phenomenon. In the case of DSC, the crystallinity is determined by relating it to the measured enthalpy changes of the system, whereas for WAXS direct information on the molecular structure is obtained by X-ray diffraction. Even for WAXS absolute values can depend on the employed method of analysis.

3.4. Dielectric Relaxation Spectroscopy (DRS). The dielectric behavior of polymers with a high degree of crystallinity like polypropylene in general follows a different nomenclature of relaxation processes as compared to amorphous polymers.[49] Figure 11 displays the dielectric behavior of pure polypropylene versus frequency and temperature in a 3D representation. The dielectric response of pure PP is weak because the asymmetry in the repeating unit of polypropylene leads only to a low dipole moment. Moreover, by oxidation processes, a small number of polar carbonyl groups can be formed. The dielectric spectra of

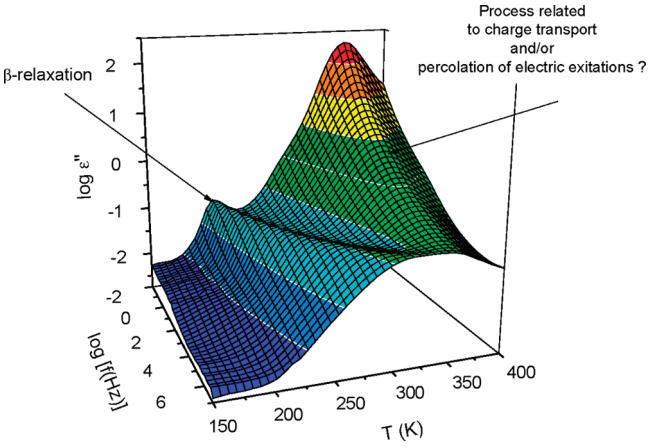

Figure 12. Dielectric behavior of the sample PP16 versus frequency and temperature in a 3D representation.

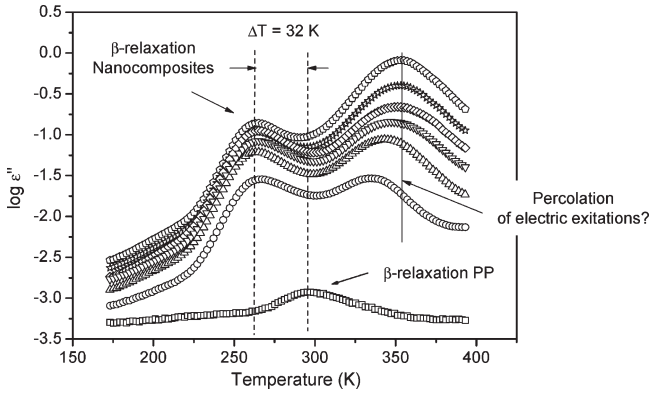

Figure 13. Dielectric loss ε'' vs temperature T at a frequency of 1 kHz for PP (squares) and different nanocomposites: PP2 (circles), PP4 (triangles), PP6 (inverted triangles), PP8 (rhombus), PP12 (stars), and PP16 (pentagons).

pure polypropylene show one main relaxation process indicated by a peak in the dielectric loss. With increasing temperature it shifts to higher frequencies as expected. This process is called β-relaxation and corresponds to the dynamic glass transition related to segmental fluctuations. At lower temperatures (higher frequencies) than the β-relaxation a γ-relaxation is observed which corresponds to localized fluctuations as discussed in more detail later.

Figure 12 shows the dielectric spectra for the nanocomposite PP16 also in a 3D representation. At lower temperature/higher frequency the β-relaxation is observed like for pure PP. Its intensity is strongly increased compared to that of pure PP. This will be discussed in detail later. At higher temperatures a further dielectrically active process is observed. This process has some specific peculiarities (see Figure 12). First, its dielectric strength decreases strongly with increasing frequency. Second, the position of the maximum of dielectric loss is independent of temperature. These characteristics indicate that this mode is not a relaxation process related to the molecular mobility of molecular dipoles, etc. It was discussed by Pissis et al. that such specific features of a dielectric process are due to percolation.[58] In a series of papers, Feldman et al. applied dielectric spectroscopy to study the percolation of electric excitations through porous silica glasses with a random structure of interconnected pores.[59−61] From the analysis of the dielectric spectra, quantitative information was deduced about the fractal nature of the pores and the porosity. In the case of the system considered here exfoliated and/or small stacks of LDH layers are present which have a huge amount of interfacial area and porosity. Therefore, these concepts of the percolation of electric excitation might also apply. Moreover, this peak disappears after heating up the sample. Therefore, it might be also due to the preparation of the nanocomposites. But a detailed discussion of conductive processes is out of scope of this work and will be published elsewhere.

Figure 13 shows the dielectric behavior of nanocomposites in the temperature domain at fixed frequency of 1 kHz in dependence on the concentration of LDH. A strong increase in the intensity of the β-relaxation with increasing concentration of LDH is observed as compared to pure PP. The increase in the measured dielectric loss with the concentration of LDH is due to an increase in the concentration of polar molecules. In the current case it is the bulky anionic surfactant (SDBS) which is the only polar component which increases with increasing concentration of LDH.[28] In the presence of a weakly polar molecule (grafted polypropylene) the polar headgroup of the SDBS ionically interacts with the surface of the LDH layer while the alkyl tail is desorbed from the layers and forms a common phase with the polypropylene segments. The polar surfactant molecules are fluctuating together with the weakly polar polypropylene segments and monitor the molecular mobility of the latter ones. Therefore, an increasing dielectric loss is observed with increasing concentration of LDH. This case is similar to the probe technique used to study the dielectric behavior of polyolefins.[62,63] In the case considered here, the SDBS molecules are predominantly located or adsorbed at the LDH layers. So DRS here probe the molecular mobility of segments located in an interfacial area close to the LDH sheets because the dielectric loss of pure polypropylene is by orders of magnitude lower and so the matrix of the nanocomposite can be regarded as dielectrically invisible. In order to prove this directly, a sample with SDBS and PP (without LDH) should be synthesized and measured. Unfortunately, no stable samples of this kind can be prepared because the SDBS molecules will migrate, aggregate, or even phase separate.

Dynamic Glass Transition (β-Relaxation). In the following, first the β-relaxation process is analyzed in detail. Compared to pure polypropylene for the nanocomposites the position of the β-relaxation is shifted by ca. 30 K to lower temperatures (see Figure 13). This leads to the conclusion that the molecular mobility in the interfacial region between the LDH layers and the matrix is higher than that in the bulk unfilled PP. This corresponds to a decreased glass transition temperature in that interfacial region compared to pure PP. Usually the model function of Haviriliak−Negami (HN)[64] is used to analyze relaxation processes quantitatively. The HN function reads

$$\varepsilon^*_{\mathrm{HN}}(f, T = \mathrm{const}) = \varepsilon_\infty + \frac{\Delta\varepsilon}{\left[1 + \left(i\frac{f}{f_{\mathrm{HN}}}\right)^{\beta}\right]^{\gamma}} \qquad (3)$$

where f_{HN} is a characteristic relaxation frequency related to the frequency of maximal loss f_{p} (relaxation rate) of the relaxation process under consideration and $\Delta\varepsilon$ is the dielectric strength. β and γ ($0 < \beta, \beta\gamma \leq 1$) are fractional parameters determining the shape of the relaxation spectra. Because of the fact that pure PP has only a weak dielectric response, it was difficult to fit the HN function in the frequency domain to the data unambiguously. For this reason, the dielectric spectra were analyzed in the

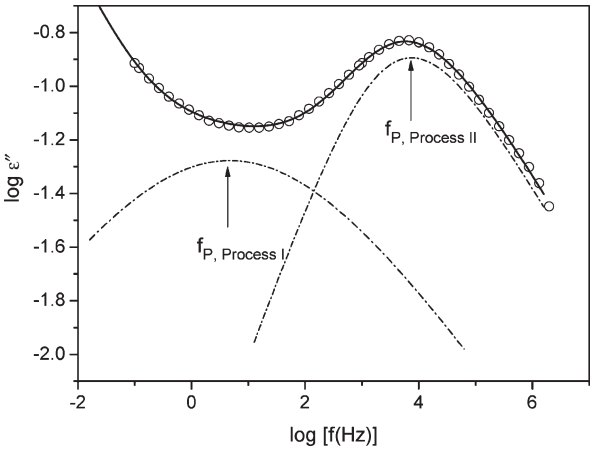

Figure 14. Dielectric loss vs frequency for the sample PP16 at $T = 273.2$ K. The solid line is a fit of two HN functions to the data including a conductivity contribution. The dashed-dotted lines correspond to individual relaxation processes. For details see text.

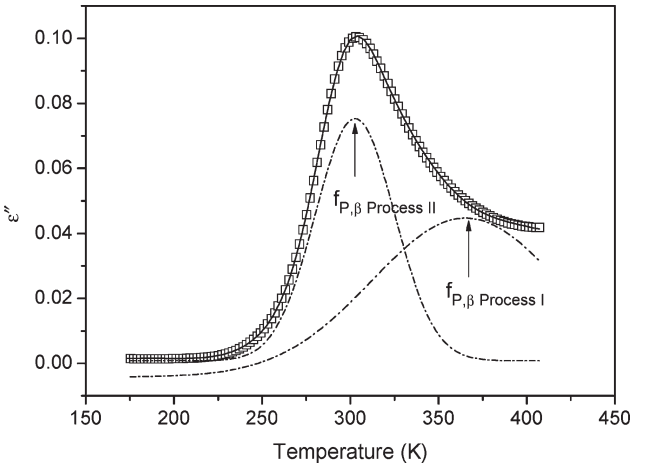

Figure 15. Dielectric loss versus temperature for the sample PP12 at a fixed frequency of 2.95×10^5 Hz. The solid line is the fit of the superposition of two Gaussians to the data were the dashed dotted lines give the individual contributions. Typical values of the regression coefficients for the fits are $r^2 = 0.999$.

temperature domain where Gaussians were fitted to the data in order to determine the mean relaxation rates at different temperatures. The method was described in detail in ref 65 and also recently applied to analyze the relaxation behavior of amorphous Ibuprofen.[66] For two relaxation processes the dielectric loss in this case can be represented as

$$\varepsilon''(T, f = \text{const}) = \sum_{i=1}^{2} a_i \exp\left(\frac{-(T - T_i^{\max})^2}{w_i}\right) + \left(\frac{\sigma_\infty}{\varepsilon_0 (2\pi f)^{mT+n}} \exp\left(\frac{-A}{T - T_0}\right)\right) + \lambda \qquad (4)$$

where a_i and $T_i^{\max}$ are the amplitude and maximum position of the Gaussian functions; w_i corresponds to the width of the peak when the intensity of the Gaussian has decreased to 1/e of the maximum value; σ_∞, A, and T_0 are the parameters that describe the conductivity dependence to the VFTH equation;[67−69] m and n are used to describe the linear dependence of the conductivity exponent on the temperature. λ is an offset. This analysis results in data pairs ($T_i^{\text{Max}} f$) which are used to construct the relaxation map. It was shown that the analysis carried out in frequency and temperature domain leads to identical results.[65,66] i counts the number of relaxation processes where for pure polypropylene one Gaussian ($i = 1$) is fitted to the data. A similar method of data analysis in temperature domain based on the HN function is published elsewhere.[70]

Figure 14 displays the dielectric loss of the nanocomposite PP16 at $T = 273.2$ K versus frequency. At higher frequencies a well-defined loss peak can be observed (see also Figure 12). A more careful inspection of this peak shows that it has a pronounced low-frequency contribution which originates from a further relaxation process. A fit of the data by only one HN function results in a parameter set with unreasonable values. In principle, the data can be described by fitting a superposition of two HN functions to the data (see Figure 14). Unfortunately, this procedure results in highly scattering parameter values especially for the frequency position of the low-frequency relaxation process. Therefore, for pure polypropylene and for the nanocomposites, the isochronal plots are analyzed where two Gaussians were fitted to the data. An example for this procedure is given in Figure 15. This strategy of data analysis leads to stable fitting results. Moreover, for pure polypropylene and its nanocomposites a consistent evaluation strategy is employed.

The two processes observed for the nanocomposites are assigned to different regions of the molecular mobility of PP segments depending on the distance from the surface of the LDH sheets.[71,72] There are only few literatures that consider adsorption of surfactant to the layers of the nanofiller. In the presence of most intercalates, the alkyl tails are desorbed from the surface of the nanoparticles and mixed with the polymer segments.[71] Room temperature NMR studies show that the disorder and the relaxation rates increase from the polar headgroup to the methyl terminus of the surfactant.[71,72] In the case considered here a similar picture is assumed. Process I appears at lower frequencies and is assigned to the PP segments in close proximity of the LDH layers. Their mobility is hindered by the strong adsorption of the polar headgroup of the surfactants at the LDH layers. A similar result is found for poly(ethylene oxide)/laponite nanocomposites by NMR.[73] Process II at higher frequencies is related to the fluctuations of the PP segments at a farer distance from the LDH sheets. Moreover, Lonkar et al. have proposed a model where the grafted units of maleic anhydride react with the sulfonate end of the surfactant.[74] This model is in line with the arguments discussed above. Moreover, it is worthy to note that a similar assignment is used to describe the relaxation behavior of PE/Mg-AL-LDH nanocomposites.[30]

The relaxation map for pure polypropylene and the corresponding nanocomposites is given in Figure 16. For each data set of the β-relaxation, the temperature dependence of the relaxation rate is curved when plotted versus $1/T$. The data can be well described by the by the VFTH equation[67−69]

$$f_p(T) = f_\infty \exp\left(\frac{-A_0}{T - T_0^{\text{id}}}\right) = f_\infty \exp\left(-\frac{DT_0^{\text{id}}}{T - T_0^{\text{id}}}\right) \qquad (5)$$

where A_0 is a constant, f_∞ is the pre-exponential factor, and T_0^{id} is the Vogel or ideal glass transition temperature. For the dynamic glass transition for T_0^{id} a value of about 30−70 K below the thermal glass transition temperature measured by DSC, etc., is

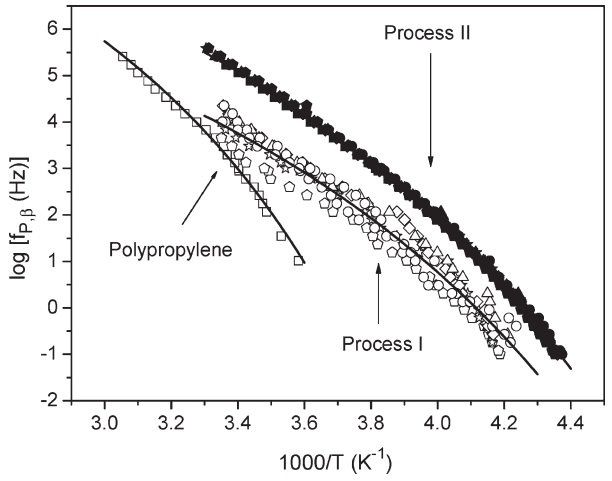

Figure 16. Relaxation rates ($f_{p,\beta}$) vs 1000/T for pure polypropylene (squares) and both the relaxation processes for the nanocomposites. Pure PP (squares), open symbols (process I) and closed symbols (process II), PP2 (circles), PP4 (triangles), PP6 (inverted triangles), PP8 (rhombus), PP12 (stars), and PP16 (pentagons). The solid lines are fits of the VFTH equation to the different data sets. For the fitting procedure see the text.

found empirically. $D = (A_0/T_0^{id})(\ln 10)$ is called fragility parameter and provides among others a useful quantity to classify glass-forming systems.[75,76] Materials are called "fragile" if their $f_p(T)$ dependence deviates strongly from an Arrhenius-type behavior and "strong" if $f_p(T)$ is close to the latter.

Figure 16 shows first that the relaxation rates of the nanocomposites collapse in the same curve for all concentrations of the nanofiller. This is true for both relaxation processes although the data for process I show a larger scatter. Second, the temperature dependence of the relaxation rate for the β-relaxation of pure polypropylene is strongly different from that for the two processes observed for the nanocomposites showing a different curvature when plotted versus $1/T$ and different values for the Vogel temperature. This indicates that a different glassy dynamics takes place for the nanocomposites in comparison to pure polypropylene. This is discussed in more detail in the following section.

For the fit of the relaxation rate by the VFTH equation a value of 12 was fixed for the pre-exponential factor to reduce the number of free fit parameter. For the nanocomposites the relaxation rates do not dependent on the concentration of the nanofiller. Therefore, for the fitting of the VFTH equation the values for all concentration were used in a common analysis. This procedure results in average values for A_0 and T_0^{id} with high statistical significance. The obtained VFT fit parameters for pure PP and processes I and II estimated for the nanocomposites are shown in Table 2.

There is a large difference in the estimated values of the VFT parameters of bulk polypropylene and that of the nanocomposites. For pure PP the molecular mobility across the whole matrix is measured, whereas for the nanocomposites the interfacial region between the LDH layers and the polypropylene matrix is selectively monitored. From the VFT parameters a dielectric glass transition temperature can be calculated for instance by $T_g^{Diel} = T$ (f_p = 10 Hz) (see Table 2). The dielectric glass transition temperature for polypropylene located in the interfacial area is by 20 K lower than that of the bulk. This downshift in T_g^{diel} is accompanied by a stronger behavior of the whole relaxation process compared to pure PP. These differences point to a

Table 2. Estimated VFT Parameters for Pure PP and Processes I and II with Fixed log [f_∞ (Hz)] = 12[a]

sample code	log [f_∞(Hz)]	A_0 (K)	T_0 (K)	T_g^{diel} (K)	D
PP	12	803	205	277	9
process I	12	1307	134 ± 5	252	22.45
process II	12	955	155 ± 2	242	14.18

[a] D is the fragility parameter, and T_g^{diel} is the dielectric glass transition temperature (see text).

difference in the physical structure of polypropylene in the bulk and polypropylene located in the interfacial area.

A more careful inspection of the estimated parameters for relaxation processes I and II reveal that there is also a difference between these two modes. The Vogel temperature of process I is 20 K lower than that of process II. Moreover process I is more fragile. These finding leads also to a 10 K higher dielectric glass transition temperature for process I. Hence, one has to conclude that the molecular dynamics in the interfacial region around the LDH sheets is also different. A temperature dependence of the relaxation rates according to the VFTH equation is regarded as a sign of glassy dynamics. Therefore, it is concluded that both the observed relaxation processes are due from a dynamic glass transition in spatial regions with different distance from the LDH layers. To have a signature as a glass transition, the spatial extent of these regions should be on the order of 1−3 nm.[77−81] So it is further concluded that the thickness or the extension of the interfacial region into the bulk matrix is about the same length scale.

The Debye theory of dielectric relaxation generalized by Kirkwood and Fröhlich gives for the dielectric relaxation strength[82]

$$\Delta\varepsilon = \frac{1}{3\varepsilon_0} g \frac{\mu^2}{k_B T} \frac{N}{V} \qquad (6)$$

where μ is the dipole moment related to the process under consideration and N/V is the number density of the dipoles involved which is proportional to C_{LDH} in case of the β-relaxation. g is the Kirkwood/Fröhlich correlation factor which describes static correlation between the dipoles. k_B is the Boltzmann's constant. The Onsager factor describing internal field effects is omitted for the sake of simplicity. ε_0 is the permittivity of free space.

The dielectric strength of the β-relaxation $\Delta\varepsilon_\beta = \varepsilon_R - \varepsilon_\infty$ is estimated as follows (see Figure 17a). The real part of the complex dielectric function is plotted versus temperatures at a fixed frequency of 1 kHz. ε_∞ is taken as value of ε' at the lowest temperatures. To minimize the influence of the high-temperature percolation process, ε_R is taken as the value of the dielectric permittivity where the dielectric loss ε'' shows the minimum between the β-relaxation and the high-temperature mode.

$\Delta\varepsilon_\beta$ is plotted versus the concentration of LDH in Figure 17b. At low concentrations of LDH the $\Delta\varepsilon_\beta$ varies linearly with C_{LDH} as expected from eq 6. This linear dependence proves the increasing number of SDBS molecules. There is a change in this linear behavior for concentrations higher than 8.95%, which may be due to some structural changes because of high loading of LDH in the polymer. For such high concentration of LDH the nanoparticle cannot arrange independently from each other. The inset of Figure 17b shows that ε_∞ is nearly constant up to same concentration of LDH and increases for PP12 and PP16, which can be taken as an additional indication for a change of the structure at higher loadings.

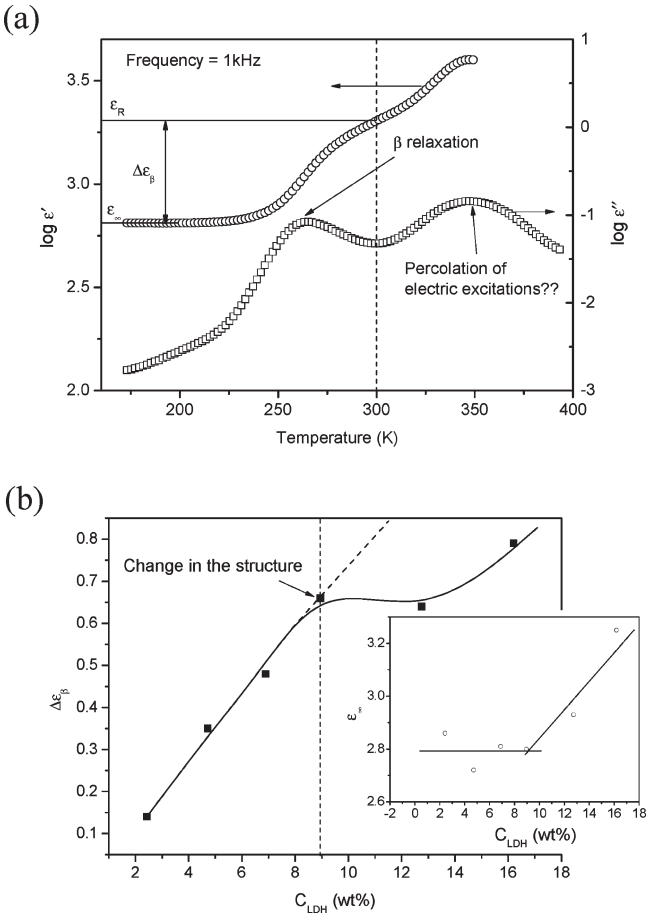

Figure 17. (a) ε' and ε'' vs temperature for PP6 at f = 1 kHz. (b) Dielectric relaxation strength $\Delta\varepsilon_\beta$ vs the concentration of LDH at f = 1 kHz. The solid line is a guide to the eyes. The dashed line indicates linear behavior $\Delta\varepsilon_\beta \sim C_{LDH}$. The inset shows the ε_∞ at lower temperatures vs C_{LDH}. The line is a guide to the eyes.

γ-Relaxation. In the temperature range between 190 and 230 K the dielectric spectra show a further relaxation process which is called γ-relaxation (Figure 18). It corresponds to the localized fluctuations within the amorphous regions. The analysis of the γ-relaxation was performed by fitting the HN function to the data. It is characterized by a symmetric peak with β values between 0.2 and 0.45. The estimated relaxation rates ($f_{p,\gamma}$) were plotted versus inverse temperature (Figure 19).

Figure 19 shows that the temperature dependence of the relaxation rate for the γ-relaxation follows the Arrhenius eq 7 as expected.

$$f_p(T) = f_\infty \exp\left(\frac{-E_A}{RT}\right) \quad (7)$$

In eq 7, E_A is the activation energy and R the universal gas constant. The relaxation rate values for all the nanocomposites are collapsing into one chart, and there is no difference due to the composition. The estimated activation energies are between 77 and 94 kJ/mol.

The γ-relaxation is a phenomenon related to the amorphous domains of the polymer matrix. From the analysis of the data the dielectric strength $\Delta\varepsilon_\gamma$ for the γ-relaxation is obtained for each concentration and plotted versus inverse temperature

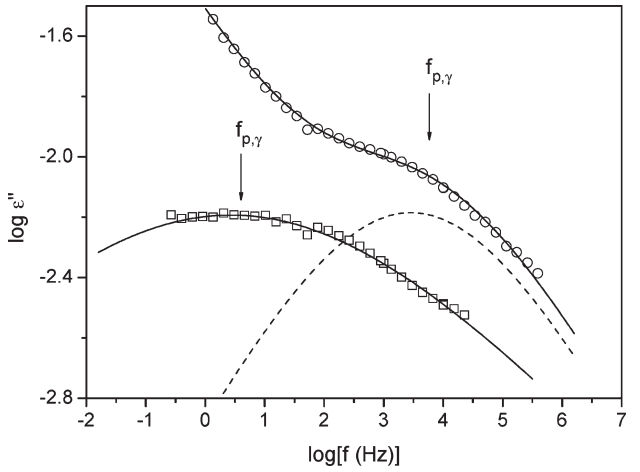

Figure 18. Dielectric loss ε'' versus frequency f showing the γ-relaxation for the sample PP16 nanocomposite at temperatures 193 K (squares) and 223 K (circles). The solid lines represent the HN fits to the data; dotted line is the contribution to the γ-relaxation at 223 K.

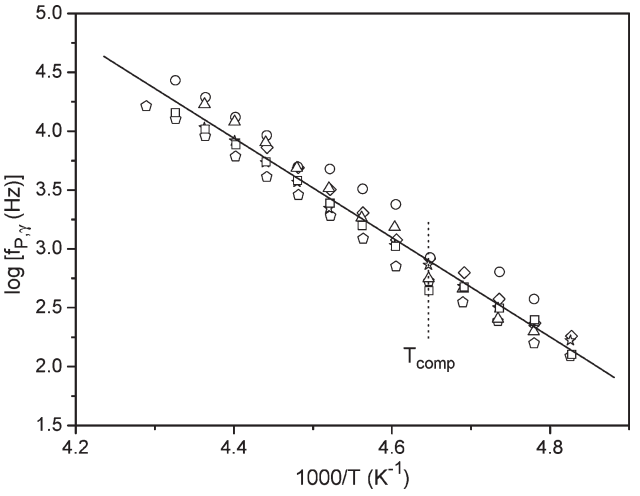

Figure 19. Relaxation rate versus inverse of the temperature for ZnAl LDH nanocomposites: PP2 (squares), PP4 (circles); PP6 (triangles), PP8 (rhombus), PP12 (stars), PP16 (pentagons). Inset shows comparison of relaxation rates as a function of LDH concentration. Solid lines are linear fit to the data.

(Figure 20). With increasing content of the nanofiller, $\Delta\varepsilon_\gamma$ increases. As discussed above, with increasing content of LDH the degree of crystallization decreases and therefore the relative amount of the amorphous phase increases. This line of argumentation is supported by the linear dependence of $\Delta\varepsilon_\gamma$ with the C_{LDH} (see Figure 21).

If the γ-relaxation occurs only in the amorphous part of the polymer, then the dielectric strength associated with this process should increase as the crystallinity decreases. An estimate of the degree of crystallinity (χ) is obtained from WAXS, which is plotted in the inset of Figure 21. The inset of Figure 21 confirms that the dielectric strength decreases as the sample becomes more amorphous. Therefore, this observation supports the hypothesis that the γ-relaxation takes place in the amorphous part of the polymer matrix.

dx.doi.org/10.1021/ma200323k |*Macromolecules* 2011, 44, 4342–4354

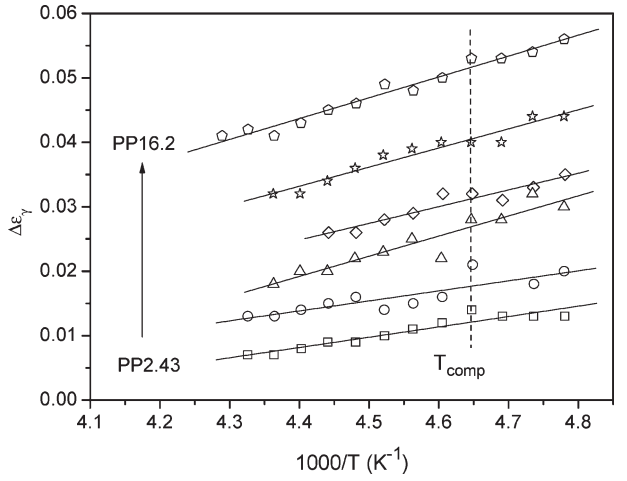

Figure 20. Dielectric strength $\Delta\varepsilon_\gamma$ versus inverse temperature for the γ-relaxation: PP2 (squares), PP4 (circles); PP6 (triangles), PP8 (inverted triangles), PP12 (stars), PP16 (pentagons). Lines are linear regressions to the corresponding data.

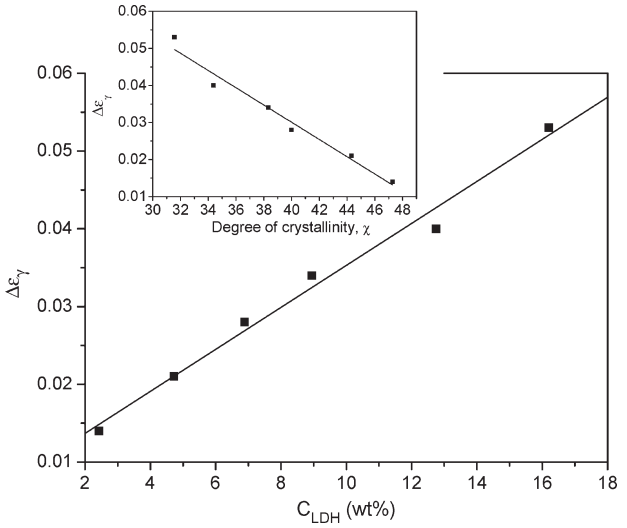

Figure 21. Dielectric strength $\Delta\varepsilon$ versus LDH concentration for the γ-relaxation of the nanocomposites at 215.5 K. The solid line is a linear regression to the data. Inset shows dielectric strength of γ-relaxation vs degree of crystallinity to the content of the polymer. The solid line is a linear regression to the data.

4. CONCLUSION

Nanocomposites are prepared in a two-step procedure by melt mixing of polypropylene and layered doubled hydroxides (LDH) where maleic anhydride grafted polypropylene is used as compatibilizer. LDH have been modified by sodium dodecylbenzenesulfonate (SDBS) as a surfactant.

The homogeneous distribution of the nanoparticles inside the polymer matrix across the whole macroscopic sample area was investigated at the synchrotron micro focus beamline μSpot (BESSY II of the Helmholtz Centre Berlin for Materials and Energy). The results show collapsing of five spectra with each other, measured with a spot of 0.1 mm at different locations over the 30 mm sample, indicating complete homogeneity of the nanocomposite.

Small-angle X-ray scattering (SAXS) analysis indicates a nearly equal stack size of O-LDH for nanocomposites as compared to pure O-LDH. It is concluded that the LDH layers in the nanocomposites are intercalated in the polymer matrix. Average number of LDH layers is calculated in the nanocomposite. The asymmetry parameter indicates a distribution of LDH stacks in different orientations in polypropylene.

The thermal properties of the nanocomposites are investigated by differential scanning calorimetry. Both the melting and crystallization enthalpies decrease with increasing concentration of LDH. Reduced to the content of the polymer the phase transition enthalpies ΔH_{Red} decreases linearly with the concentration of the nanofiller. The extrapolation of ΔH_{Red} to zero leads to a limiting concentration of ca. 40 wt % LDH where the crystallization should be completely suppressed by the presence of the nanoparticles.

The dielectric loss of pure polypropylene is weak, but several relaxation processes can be indentified: a β-relaxation which corresponds to the dynamic glass transition due to cooperative segmental fluctuations and a γ-process at low temperatures which corresponds to localized fluctuations in the amorphous parts of polypropylene.

The intensity of the β-relaxation (dynamic glass transition) increases strongly with increase in concentration of LDH for the nanocomposites. This increase in the dielectric relaxation strength of the dynamic glass transition is related to the increase in the concentration of the quite polar SDBS surfactant molecules which increases with the concentration of LDH. The surfactants are adsorbed onto the LDH layers, and its alkyl tails form a common phase with the polypropylene segments close to the nanoparticles. Therefore, a detailed investigation of the β-relaxation provides information about the molecular mobility and structure in the interfacial area between the LDH layers and the matrix polymer. It was shown that the peak of the β-relaxation consist of two processes. These processes are assigned from regions of different molecular mobility at different distances from the LDH nanofillers. The temperature dependence of the relaxation rates of both processes follows the Vogel−Fulcher−Tammann−Hesse formula which indicates glassy dynamics. The difference in the corresponding glass temperatures measured by the ideal glass transition or Vogel temperature T_0 is about 20 K. The low-frequency component of the β-relaxation of the nanocomposites is assigned to polypropylene segments in a close proximity of the LDH because the SDBS molecules are strongly adsorbed at the surfaces of the nanofiller and have therefore a strongly reduced molecular mobility. The high frequency process of the β-relaxation is related to polypropylene segments at a distance farther from the LDH layers. The higher molecular mobility is caused by a plasticization of the alkyl tail of the SDBS surfactants terminated with a methyl group. The concentration dependence of the dielectric strength for the β-relaxation changes strongly for a loading higher than 10 wt %. This is probably due to the fact that for high filler concentrations the LDH sheets (or small LDH stacks) cannot arrange independently from each other. Therefore, on optimal filler loading can be deduced from that dependence to be below 10 wt %.

The temperature dependence of the relaxation rates of the γ-relaxation follows the Arrhenius equation with activation energy of around 81 kJ/mol, independent of the concentration of LDH. The relaxation strength of the γ-process increases with the concentration of the nanofiller. Because the γ-relaxation is related to localized fluctuation in the amorphous regions of polypropylene, it is concluded that the content of the amorphous

phase increases with increasing concentration of LDH. This is confirmed by a linear dependence of $\Delta\varepsilon_\gamma$ on the roughly estimated degree of crystallization.

AUTHOR INFORMATION

Corresponding Author

*Tel: +49 30/8104-3384. Fax: +49 30/8104-1637. E-mail: Andreas.Schoenhals@bam.de. For chemistry and preparation please contact D.-Y. W., E-mail: deyiwang@scu.edu.cn

ACKNOWLEDGMENT

The authors gratefully acknowledge the assistance of Ms. S. Rolf and Mr. D. Neubert for their experimental help. The financial support from the Ph.D. program of BAM (to P.J.P.) and from Alexander von Humboldt Foundation (to D.-Y.W.) is highly appreciated.

REFERENCES

(1) LeBaron, P. C.; Wang, Z.; Pinnavaia, T. J. *Appl. Clay Sci.* **1999**, *15*, 11.

(2) Novak, B. M. *Adv. Mater.* **1993**, *5*, 422.

(3) Alexandre, M.; Dubois, P. *Mater. Sci. Eng.* **2000**, *28*, 1.

(4) Krishnamoorti, R.; Vaia, R. A. *Polymer Nanocomposites*; ACS Symp. Ser. Vol. 804; American Chemical Society: Washington, DC, 2002.

(5) Ray, S. S.; Okamoto, M. *Prog. Polym. Sci.* **2003**, *28*, 1539.

(6) Nalwa, H. S. *Handbook of Organic-Inorganic Hybrid Materials and Nanocomposites*; American Scientific Publishers: Stevenson Ranch, CA, 2003; Vol. 2.

(7) Leuteritz, A.; Kretzschmar, B.; Pospiech, D.; Costa, R. F.; Wagenknecht, U.; Heinrich, G. Industry-relevant preparation, characterization and applications of polymer nanocomposites. In *Polymeric Nanostructures and Their Applications*; Nalwa, H. S., Ed.; American Scientific Publishers: Los Angeles, 2007.

(8) Vaia, R. A.; Giannelis, E. P. *MRS Bull.* **2001**, *26*, 394.

(9) Davis, S. R.; Brough, A. R.; Atkinson, A. *J. Non-Cryst. Solids* **2003**, *315*, 197.

(10) Fragiadakis, D.; Pissis, P.; Bokobza, L. *Polymer* **2005**, *46*, 6001.

(11) Hooper, J. B.; Schweitzer, K. S. *Macromolecules* **2005**, *38*, 8850.

(12) Böhning, M.; Goering, H.; Fritz, A.; Brzezinka, K. W.; Turky, G.; Schönhals, A.; Schartel, B. *Macromolecules* **2005**, *38*, 2764.

(13) Jancar, J.; Douglas, J. F.; Starr, F. W.; Kumar, S. K.; Cassagnau, P.; Lesser, A. J.; Sternstein, S. S.; Buehler, M. J. *Polymer* **2010**, *51*, 3321.

(14) Hussain, F.; Hojjati, M.; Okamoto, M.; Gorga, R. E. *J. Compos. Mater.* **2007**, *40*, 1511.

(15) Giannelis, E. P.; Krishnamoorti, R.; Manias, E. *Adv. Polym. Sci.* **1999**, *138*, 107.

(16) Giannelis, E. P. *Adv. Mater.* **1996**, *8*, 29.

(17) Gilman, J. W.; Jackson, C. L.; Morgan, A. B.; Harris, R., Jr. *Chem. Mater.* **2000**, *12*, 1866.

(18) Ray, S. S. *J. Ind. Eng. Chem.* **2006**, *12*, 811.

(19) Heilmann, A. *Polymer Films with Embedded Metal Nanoparticles*: Springer: Berlin, 2003.

(20) Xie, X. L.; Mai, Y. W.; Zhou, X. P. *Mater. Sci. Eng. Res.* **2005**, *49*, 89.

(21) Bernholc, J.; Brenner, D.; Nardelli, M. B.; Meunier, V.; Roland, C. *Annu. Rev. Mater. Res.* **2002**, *32*, 347.

(22) Moniruzzaman, M.; Winey, K. I. *Macromolecules* **2006**, *39*, 5194.

(23) Lichtenhan, J. D.; Schwab, J. J.; Reinerth, W. A. *Chem. Innov.* **2001**, *31*, 3.

(24) Joshi, M.; Butola, B. S. *J. Macromol. Sci., Polym. Rev.* **2004**, *C44*, 389.

(25) Hao, N.; Böhning, M.; Goering, H.; Schönhals, A. *Macromolecules* **2007**, *40*, 2955.

(26) Hao, N.; Böhning, M.; Schönhals, A. *Macromolecules* **2007**, *40*, 9672.

(27) Hao, N.; Böhning, M.; Schönhals, A. *Macromolecules* **2010**, *43*, 9417.

(28) Costa, F. R.; Saphiannikova, M.; Wagenknecht, U.; Heinrich, G. *Adv. Polym. Sci.* **2008**, *210*, 101.

(29) Kovanda, F.; Jindova, E.; Lang, K.; Kubat, P.; Sedlakova, Z. *Appl. Clay Sci.* **2010**, *48*, 260.

(30) Schönhals, A.; Goering, H.; Costa, F. R.; Wagenknecht, U.; Heinrich, G. *Macromolecules* **2009**, *42*, 4165.

(31) Tichit, D.; Coq, B. *CATTECH* **2003**, *7*, 206.

(32) Frunza, L.; Schönhals, A.; Frunza, S.; Parvulescu, V. I.; Cojocaru, B.; Carriazo, D.; Martín, C.; Rives, V. *J. Phys. Chem. A* **2007**, *111*, 5166.

(33) van der Ven, L.; Van Gemert, M. L. M.; Batenburg, L. F.; Keern, J. J.; Gielgens, L. H.; Koster, T. P. M.; Fischer, H. R. *Appl. Clay Sci.* **2000**, *17*, 25.

(34) Du, L.; Qu, B.; Zhang, M. *Polym. Degrad. Stab.* **2007**, *92*, 497.

(35) Wang, D. Y.; Das, A.; Costa, F. R.; Leuteritz, A.; Wagenknecht, U.; Heinrich, G. *Langmuir* **2010**, *26*, 14162.

(36) Wang, D. Y.; Leuteritz, A.; Wang, Y. Z.; Wagenknecht, U.; Heinrich, G. *Polym. Degrad. Stab.* **2010**, *95*, 2474.

(37) Davis, R. D.; Bur, A. J.; McBrearty, M.; Lee, Y. H.; Gilman, J. W.; Start, P. R. *Polymer* **2004**, *45*, 6487.

(38) Ding, Y.; Pawlus, S.; Sokolov, A. P.; Douglas, J. F.; Karim, A.; Soles, C. L. *Macromolecules* **2009**, *42*, 3201.

(39) Anastasiadis, S. H.; Karatasos, K.; Vlachos, G.; Manias, E.; Gianneis, E. P. *Phys. Rev. Lett.* **2000**, *84*, 915.

(40) Schwartz, G. A.; Bergman, R.; Swenson, J. *J. Chem. Phys.* **2004**, *120*, 5736.

(41) Mijovic, J.; Lee, H. K.; Kenny, J.; Mays, J. *Macromolecules* **2006**, *39*, 2172.

(42) Elmahdy, M. M.; Chrissopoulou, K.; Afratis, A.; Floudas, G.; Anastasiadis, S. H. *Macromolecules* **2006**, *39*, 5170.

(43) Kopesky, E. T.; Haddad, T. S.; McKinley, G. H.; Cohen, R. E. *Polymer* **2005**, *46*, 4743.

(44) Cole, K. C. *Macromolecules* **2008**, *41*, 834.

(45) Wurm, A.; Ismail, M.; Kretzschmar, B.; Pospiech, D.; Schick, C. *Macromolecules* **2010**, *43*, 1480.

(46) Bandyopadhyay, J.; Ray, S. S. *Polymer* **2010**, *51*, 1437.

(47) Preschilla, N.; Sivalingam, G.; Abdul Rasheed, A. S.; Tyagi, S.; Biswas, A.; Bellare, J. *Polymer* **2008**, *49*, 4285.

(48) Zhu, X.; Melian, C.; Dou, Q.; Peter, K.; Demco, D. E.; Möller, M.; Anokhin, D. V.; Marc Le Meins, J.; Ivanov, D. A. *Macromolecules* **2010**, *43*, 6067.

(49) Schönhals, A. Molecular Dynamics in Polymer Model Systems. In *Broadband Dielectric Spectroscopy*; Kremer, F., Schönhals, A., Eds.; Springer: Berlin, Germany, 2002; p 35.

(50) Kremer, F.; Schönhals, A. Broadband Dielectric Measurement Techniques. In *Broadband Dielectric Spectroscopy*; Kremer, F., Schönhals, A., Eds.; Springer: Berlin, Germany, 2002; p 35.

(51) Paris, O.; Li, C.; Siegel, S.; Weseloh, G.; Emmerling, F.; Riesemeier, H.; Erko, A.; Fratzl, P. *J. Appl. Crystallogr.* **2007**, *40*, S466.

(52) Hammersley, A. P.; Svensson, S. O.; Hanfland, M.; Fitch, A. N.; Hausermann, D. *High Pressure Res.* **1996**, *14*, 235.

(53) Burum, D. P.; Rhim, W. K. *J. Phys. Chem.* **1979**, *71*, 944.

(54) Wang, D. Y.; Costa, F. R.; Vyalikh, A.; Leuteritz, A.; Scheler, U.; Jehnichen, D.; Wagenknecht, U.; Häussler, L.; Heinrich., G. *Chem. Mater.* **2009**, *21*, 4490.

(55) Lonjon, A.; Laffont, L.; Demont, P.; Dantras, E.; Lacabanne, C. *J. Phys. D: Appl. Phys.* **2010**, *43*, 345401.

(56) Hommingа, D.; Goderis, B.; Dolbnya, I.; Groeninckx, G. *Polymer* **2006**, *47*, 1620.

(57) Miltner, H. E.; Grossiord, N.; Lu, K.; Loos, J.; Koning, C. E.; van Mele, B. *Macromolecules* **2008**, *41*, 5753.

(58) Pissis, P.; Laudat, J.; Daoukaki, D.; Kyritsis, A. *J. Non-Cryst. Solids* **1994**, *171*, 201.

(59) Puzenko, A.; Kozlovich, N.; Gutina, A.; Feldman, Y. *Phys. Rev. B* **1999**, *60*, 14349.
(60) Gutina, A.; Antropova, T.; Rysiakiewicz-Pasek, E.; Virnik, K.; Feldman, Y. *Microporous Mesoporous Mater.* **2003**, *58*, 237.
(61) Feldman, Y.; Puzenko, A.; Ryabov, Y. *Chem. Phys.* **2003**, *284*, 139.
(62) van den Berg, O.; Wübbenhorst, M.; Picken, S. J.; Jager, W. F. *J. Non-Cryst. Solids* **2005**, *351*, 2694.
(63) van den Berg, O.; Sengers, W. G. F.; Jager, W. F.; Picken, S. J.; Wübbenhorst, M. *Macromolecules* **2004**, *37*, 2460.
(64) Havriliak, S.; Negami, S. *Polymer* **1967**, *8*, 161.
(65) Hartmann, L.; Pouret, P.; Leger, L.; Kremer, F. *J. Chem. Phys.* **2003**, *118*, 6052.
(66) Brás, A. R.; Noronha, J. P.; Antunes, A. M. M.; Cardoso, M. M.; Schönhals, A.; Affouard, F.; Dionísio, M.; Correia, N. T. *J. Phys. Chem. B* **2008**, *112*, 11087.
(67) Vogel, H. *Phys. Z.* **1921**, *22*, 645.
(68) Fulcher, G. S. *J. Am. Ceram. Soc.* **1925**, *8*, 339.
(69) Tammann, G.; Hesse, W. *Z. Anorg. Allg. Chem.* **1926**, *156*, 245.
(70) Schlosser, E.; Schönhals, A.; Carius, H. E.; Goering, H. *Macromolecules* **1993**, *26*, 6027.
(71) Jacobs, J. D.; Koerner, H.; Heinz, H.; Farmer, B. L.; Mirau, P.; Garrett, P. H.; Vaia, R. A. *J. Phys. Chem. B* **2006**, *110*, 20143.
(72) Kubies, D.; Jérôme, R.; Grandjean, J. *Langmuir* **2002**, *18*, 6159.
(73) Lorthioir, C.; Lauprêtre, F.; Soulestin, J.; Lefebvre, J.-M. *Macromolecules* **2009**, *42*, 218.
(74) Lonkar, S. P.; Morlat-Therias, S.; Caperaa, N.; Leroux, F.; Gardette, J. L.; Singh, R. P. *Polymer* **2009**, *50*, 1505.
(75) Angell, C. A. *J. Non-Cryst. Solids* **1991**, *13*, 131.
(76) Angell, C. A. *J. Res. Natl. Inst. Stand. Technol.* **1997**, *102*, 171.
(77) Donth, E. *J. Non-Cryst. Solids* **1982**, *53*, 325.
(78) Hempel, E.; Hempel, G.; Hensel, A.; Schick, C.; Donth, E. *J. Phys. Chem. B* **2000**, *104*, 2460.
(79) Sills, S.; Gray, T.; Overney, R. M. *J. Chem. Phys.* **2005**, *123*, 134902.
(80) Berthier, L.; Biroli, G.; Bouchaud, J. P.; Cipelletti, L.; El Masri, D.; L'Hote, D.; Ladieu, F.; Pierno, M. *Science* **2005**, *310*, 1797.
(81) Cangialosi, D.; Alegria, A.; Colmenero, J. *Phys. Rev. E* **2007**, *76*, 011514.
(82) Schönhals, A.; Kremer, F. *Theory of Dielectric Relaxation Spectra in Broadband Dielectric Spectroscopy*; Kremer, F., Schönhals, A., Eds.; Springer: Berlin, 2002; p 1.